ELSEVIER

Surface Science 513 (2002) 468–474

SURFACE SCIENCE

www.elsevier.com/locate/susc

Absolute orientation-dependent TiN(0 0 1) step energies from two-dimensional equilibrium island shape and coarsening measurements on epitaxial TiN(0 0 1) layers

S. Kodambaka *, S.V. Khare, V. Petrova, A. Vailionis [1], I. Petrov, J.E. Greene

Department of Materials Science and the Frederick Seitz Materials Research Laboratory, University of Illinois, 104 South Goodwin Avenue, Urbana, IL 61801, USA

Received 18 April 2002; accepted for publication 14 May 2002

Abstract

In situ high-temperature (1030–1223 K) scanning tunneling microscopy was used to determine the equilibrium shapes of two-dimensional TiN vacancy islands on atomically smooth terraces of epitaxial TiN(0 0 1) layers. Inverse Legendre transformations of the equilibrium island shapes yield relative step energies as a function of step orientation within an orientation-independent scale factor λ, the equilibrium chemical potential of the island per unit TiN molecular area. We then use quantitative TiN(0 0 1) adatom island coarsening measurements to determine λ and, hence, absolute orientation-dependent step energies β and step stiffnesses $\tilde{\beta}$. For $\langle 1\,1\,0\rangle$ and $\langle 1\,0\,0\rangle$ steps on TiN(0 0 1), we obtain: $\beta_{1\,1\,0} = 0.21 \pm 0.05$ eV/Å, $\beta_{1\,0\,0} = 0.25 \pm 0.05$ eV/Å, $\tilde{\beta}_{1\,1\,0} = 0.9 \pm 0.2$ eV/Å, and $\tilde{\beta}_{1\,0\,0} = 0.07 \pm 0.02$ eV/Å. From the $\tilde{\beta}$ values, we calculate kink formation energies $\varepsilon_{1\,1\,0} = 0.40 \pm 0.2$ eV and $\varepsilon_{1\,0\,0} = 0.11 \pm 0.1$ eV based on the unrestricted terrace-step-kink model.

Keywords: Surface diffusion; Surface thermodynamics (including phase transitions); Scanning tunneling microscopy; Models of surface kinetics; Clusters; Single crystal surfaces; Adatoms

B1 NaCl-structure TiN is widely used for depositing hard wear-resistant coatings on cutting tools, diffusion-barrier layers in microelectronic devices, corrosion-resistant coatings on mechanical devices, and abrasion-resistant layers on optical components. Even though the elastic and diffusion-barrier properties of TiN are highly anisotropic, and hence depend strongly upon film texture, the mechanisms and reaction paths leading to the development of preferred orientation in polycrystalline TiN layers are not understood. Efforts to model these processes [1] require, as input, detailed knowledge of adatom transport and surface site energies. Relatively little information is available concerning these parameters. Some progress has been made recently toward obtaining adatom transport parameters on TiN(0 0 1) and

* Corresponding author. Address: Materials Science and Engineering, 1101 W. Springfield Avenue, ESB 1-131, Urbana, IL 61801, USA. Tel.: +1-217-3337080; fax: +1-217-2441638.

E-mail addresses: kodambak@uiuc.edu (S. Kodambaka), arturas@stanford.edu (A. Vailionis).

[1] Present address: Geballe Laboratory for Advanced Materials, McCullough Bldg. 227, 476 Lomita Mall, Stanford University, Stanford, CA 94305, USA.

0039-6028/02/$ - see front matter
PII: S0039-6028(02)01845-9

(1 1 1) surfaces [2–4]. Here, we focus on the determination of absolute step formation energies on TiN(0 0 1).

The step formation energy β as a function of step orientation φ is a fundamental parameter used to describe crystal surfaces. $\beta(\varphi)$ is the two-dimensional (2D) analog of the surface free energy $\gamma(\varphi)$. Just as $\gamma(\varphi)$ determines the equilibrium shape of bulk crystals, the variation of β with φ determines the equilibrium shape of 2D islands on a terrace. A related property, the step-edge stiffness, $\tilde{\beta}(\varphi) \equiv \beta(\varphi) + \mathrm{d}^2\beta(\varphi)/\mathrm{d}\varphi^2$, is proportional to the island chemical potential [5] and hence controls island coarsening and decay kinetics.

Experimental determination of orientation-dependent step energies is difficult. Methods involving a combination of 2D island equilibrium shape and step fluctuation measurements [6], 3D equilibrium crystal shape and surface energy [7], temperature-dependence of 2D island equilibrium shapes [8,9], and anisotropic island shape fluctuations [10] have been used to determine absolute step energies. *Orientation-averaged* step energies have been determined from near-isotropic island shape fluctuations [11] and 2D island coarsening measurements [12,13]. However, methods described in Refs. [12] and [13] alone are not applicable to determine absolute orientation-dependent step energies for anisotropic island shapes.

In this letter, we present an approach, based upon measurements of the equilibrium island shape combined with island coarsening analyses, for the determination of absolute $\beta(\varphi)$ values on atomically smooth TiN(0 0 1) terraces using in situ high-temperature scanning tunneling microscopy (STM). We use an analytical expression for the orientation dependence of $\beta(\varphi)$ from the equilibrium shape using the inverse Legendre transformation procedure described in Ref. [10]. This provides relative $\beta(\varphi)$ values within an orientation-independent scale factor λ, the equilibrium island chemical potential per unit TiN molecular area, while eliminating the conventional inverse Wulff-construction which involves the tedious procedure of tangent constructions. Next, we use in situ high-temperature STM measurements of TiN(0 0 1) adatom island coarsening (Ostwald ripening) on atomically smooth TiN(0 0 1) terraces to determine λ and, hence, absolute values for $\beta(\varphi)$.

Epitaxial TiN(0 0 1) layers, 3000 Å thick, were grown on MgO(0 0 1) by ultra-high vacuum (UHV) magnetically unbalanced magnetron sputter deposition [14] using the procedure described in Ref. [15]. The samples were transferred to a UHV multichamber system, with a base pressure of 2×10^{-10} Torr, containing a variable-temperature Omicron STM. The system is equipped with facilities for electron-beam evaporation, ion etching, Auger electron spectroscopy (AES), and low energy electron diffraction (LEED). Sample temperatures were measured by optical pyrometry and calibrated using temperature-dependent TiN emissivity data obtained by spectroscopic ellipsometry.

The TiN(0 0 1) layers were degassed in UHV at 1073 K, where the N_2 vapor pressure over TiN is less than 10^{-10} Torr [16], for approximately 20 min. Epitaxial TiN(0 0 1) buffer layers, 50–100 Å thick, were then deposited at 1023 K in the STM chamber by reactive evaporation from Ti rods (99.999% purity) in N_2 (99.999%) at 1×10^{-7} Torr. The buffer layers were annealed in N_2 for 4 h at temperatures $T_a \simeq 1100$ K. This procedure results in sharp 1×1 LEED patterns corresponding to an in-plane atomic spacing of 4.24 Å and an STM-measured step height of 2.12 Å, both equal to expected values for bulk TiN [17]. AES analyses show that the samples contain $\simeq$2 mol% oxygen, probably in the form of TiO which is isostructural [17] and mutually soluble with TiN. STM images reveal that the layer surfaces consist of terraces 400–800 Å wide, depending upon T_a, separated by single-atom-high steps.

Partial TiN monolayers (ML) with coverages 0.1–0.8 ML were deposited on the TiN/MgO(0 0 1) substrates by reactive evaporation at room temperature. The partial monolayer samples were annealed in N_2 at $T_a = 1023$–1223 K while scanning the surface in the STM. This resulted in a distribution of square-shaped TiN(0 0 1) 2D adatom islands of average radii 15–40 Å at coverages $<$0.4 ML and vacancy islands of average radii 60–160 Å at higher coverages. Using a combination of LEED and STM measurements, we find that the islands are bounded by $\langle 1\,1\,0 \rangle$ steps.

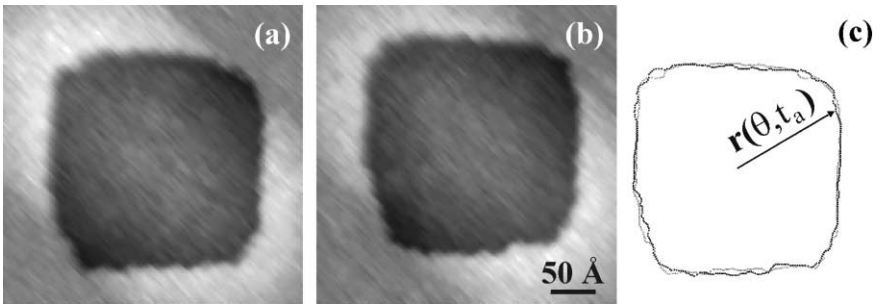

Fig. 1. (a,b) Consecutive STM images (338 × 338 Å^2) of a 2D TiN(0 0 1) vacancy island on an atomically smooth TiN(0 0 1) surface. The images were acquired at 15 s/frame during annealing at $T_a = 1140$ K. (c) Corresponding outlines $r(\theta, t_a)$ of the island shapes.

Prior to obtaining the in situ temperature-dependent STM data reported below, the sample and tip were allowed to stabilize thermally at T_a for 2–3 h. At each T_a, STM images of individual vacancy islands were continuously acquired at a rate of 12–44 s/frame for annealing times t_a up to 60 min. Pixel resolution varied from 0.75×0.75 to 2.5×2.5 Å^2. Typical tunneling conditions were 0.6 nA at 0.8–2.0 V. Scan sizes, scan rates, and tunneling parameters were varied to check for tip induced effects. No such effects were observed in results presented here.

For each of the measurement sequences, island boundaries and areas A were determined from the STM images using Image SXM, an image processing software [18]. To determine the equilibrium island shape, we require islands of constant area. Thus, the boundary coordinates $r(\theta, t_a)$ of measured islands, of average radii >100 Å, were normalized to the smallest island area in the measurement sequence following the procedure used in Ref. [10]. The equilibrium island shape $R(\theta)$ was then obtained by averaging $r(\theta, t_a)$ at all t_a values within the measurement sequence. [2]

Figs. 1a and 1b are typical results showing consecutive STM images of a TiN(0 0 1) 2D vacancy island acquired at 1140 K while scanning at 15 s/frame. The corresponding island outlines, $r(\theta, t_a)$, are presented in Fig. 1c. Equilibrium island shapes $R(\theta)$, determined from 62 images using the procedure described above, were fit with Lorentzian functions [3] of general form,

$$R = R_o + \frac{a}{[1 + b(\theta - \theta_c)^2]}, \quad (1)$$

where R_o, a, b, and θ_c are fitting parameters. R vs. θ for the island corresponding to Fig. 1 is plotted in Fig. 2a. The open circles represent the measured data while the solid line is the analytical fit obtained using Eq. (1). All experimental data were equally well fit.

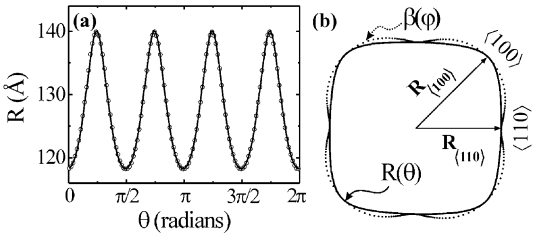

Fig. 2. (a) Plot of R vs. θ for the TiN(0 0 1) island shown in Fig. 1. Open circles represent experimental data and the solid line is the analytical fit obtained using Eq. (1). (b) Polar plots of R vs. θ and β vs. φ determined using Eqs. (2a) and (2b) with $\lambda = 1$.

[2] The average island shape $\overline{R}(\theta) = \langle r(\theta, t_a) \rangle$ was found to be distorted, with assymmetric ⟨1 1 0⟩ step-edge lengths, due to hysteresis [8] in the STM piezo-electric actuators. The distorted shape $\overline{R}(\theta)$ was transformed to the symmetric equilibrium island shape $R(\theta)$ using the fourfold symmetry of the TiN(0 0 1) lattice and imposing the condition $R(\theta_i + n\pi/2) \equiv (1/4) \times \sum_{n=0,1,2,3} \overline{R}(\theta_i + n\pi/2)$ for θ_i values between 0 and $\pi/2$.

[3] Measured $R(\theta)$ data at θ values over the range 0–$\pi/2$ were fit with two Lorentzian functions. The same set of functions, with θ_c shifted by $\pi/2$, π, and $3\pi/2$, were used to fit the data at higher θ values. The form of Eq. (1), which provides an analytical means to calculate $\dot{R}$ and $\ddot{R}$, has no physical significance.

The inverse Legendre transform of $R(\theta)$ yields relative values of $\beta(\varphi)$ through the analytical expression [10]

$$\beta(\varphi) = \lambda \frac{[R(\theta)]^2}{\sqrt{[R(\theta)]^2 + [\dot{R}(\theta)]^2}}, \tag{2a}$$

with

$$\varphi = \theta - \arctan(\dot{R}/R), \tag{2b}$$

where $\dot{R}$ is the first spatial derivative of R with respect to θ. A polar plot of $\beta(\varphi)$ (dotted line) calculated with $\lambda = 1$ is shown in Fig. 2b in which the straight and corner steps are $\langle 1\,1\,0\rangle$ and $\langle 1\,0\,0\rangle$, respectively. The ratio of step energies, $\beta_{1\,1\,0}/\beta_{1\,0\,0}$ (i.e., the maximum variation of β with φ) obtained using Eqs. (2a) and (2b) is 0.84. However, in order to obtain absolute $\beta(\varphi)$ values, λ in Eq. (2a) has to be determined independently. We do this using the island coarsening (Ostwald ripening) experiments described below.

Ostwald ripening is a phenomenon in which larger islands grow at the expense of smaller ones and is described by the Gibbs–Thomson equation [5,19]

$$\rho^{\mathrm{eq}} = \rho_{\infty}^{\mathrm{eq}} \exp\left(\frac{\beta\Omega}{\tilde{r}kT_{\mathrm{a}}}\right), \tag{3}$$

where ρ^{eq} is the equilibrium free adatom concentration associated with an island of radius $\tilde{r}$, $\rho_{\infty}^{\mathrm{eq}}$ is the equilibrium free adatom concentration associated with a straight step, and Ω is the unit TiN molecular area. Note that Eq. (3), while commonly used in the literature to represent the Gibbs–Thomson equation, is specific to the case of isotropic (circular) islands. The general equation for anisotropic (non-circular) equilibrium island shapes is

$$\rho^{\mathrm{eq}} = \rho_{\infty}^{\mathrm{eq}} \exp\left(\frac{\tilde{\beta}(\varphi)\kappa(\theta)\Omega}{\mathrm{kT_a}}\right). \tag{4}$$

$\kappa(\theta)$ in Eq. (4) is the curvature of the equilibrium island shape given by the relation

$$\kappa(\theta) = \frac{S(\theta)}{R_{\mathrm{avg}}}, \tag{5a}$$

where

$$S(\theta) = \frac{\left\{[R(\theta)/R_{\mathrm{avg}}]^2 + 2[\dot{R}(\theta)/R_{\mathrm{avg}}]^2 - [R(\theta)\ddot{R}(\theta)/R_{\mathrm{avg}}^2]\right\}}{\left\{[R(\theta)/R_{\mathrm{avg}}]^2 + [\dot{R}(\theta)/R_{\mathrm{avg}}]^2\right\}^{3/2}} \tag{5b}$$

is a dimensionless orientation-dependent curvature function describing the equilibrium shape and $R_{\mathrm{avg}} = \sqrt{A/\pi}$ is the average island radius. [4] $\ddot{R}$ in Eq. (5b) denotes the second spatial derivative of R with respect to θ. The step-edge stiffness $\tilde{\beta}(\varphi)$ is related to $\kappa(\theta)$ through the expression [5,10,20]

$$\tilde{\beta}(\varphi) = \frac{\lambda}{\kappa(\theta)}. \tag{6}$$

λ, the equilibrium chemical potential of the island per unit TiN molecular area, in Eq. (6), is independent of step orientation and depends only on island size. Thus, by combining Eqs. (5a), (5b), and (6), we obtain an exact expression for λ in terms of the *orientation-independent* parameters R_{avg} and B:

$$\lambda = \frac{B}{R_{\mathrm{avg}}}, \tag{7a}$$

with

$$B \equiv \tilde{\beta}(\varphi)S(\theta). \tag{7b}$$

B, defined in Eq. (7b), determines the energy scale of the surface equilibrium chemical potential. (Giesen and co-workers [13,21] derived a similar expression for λ in terms of shape factors which is exact for anisotropic islands at 0 K. However, the present expression is valid at any temperature.) For the case of circular islands, $B = \beta$ and $R_{\mathrm{avg}} = \tilde{r}$, and we recover Eq. (3). For the case of anisotropic equilibrium island shapes, Eq. (4) can be written in terms of B and R_{avg}, as

$$\rho^{\mathrm{eq}} = \rho_{\infty}^{\mathrm{eq}} \exp\left(\frac{B\Omega}{R_{\mathrm{avg}}kT_{\mathrm{a}}}\right). \tag{8}$$

[4] R_{avg} can also be defined as $R_{\mathrm{avg}} = \frac{1}{2\pi}\int_0^{2\pi} \mathrm{d}\theta R(\theta)$ which would lead to a slightly different value of B. This however, has no effect on the value of λ, and hence β values, obtained by this analysis.

We have used in situ high-temperature STM to follow 2D adatom island coarsening kinetics on TiN(0 0 1) surfaces, where the rate-limiting mechanism is surface diffusion [2], and Eq. (8) to model the results in order to obtain B and, hence, λ. To extract B from time- and temperature-dependent STM measurements, we have chosen a simple experimental geometry, an adatom island placed in a vacancy pit, where the equilibrium free adatom concentrations around the island are well defined. The decay rate $\mathrm{d}A/\mathrm{d}t_a$ of an island in this geometry is given by [22]

$$\frac{\mathrm{d}A}{\mathrm{d}t_a} = -2\pi\Omega C\rho_\infty^{eq} \times \left[\exp\left(\frac{B\Omega}{R_{avg}kT_a}\right) - \exp\left(-\frac{B\Omega}{R_p kT_a}\right)\right], \quad (9)$$

where the proportionality constant C is a temperature-dependent rate coefficient and R_p is the average radius of the vacancy pit.

We model diffusion-limited island decay kinetics for this configuration using an adaptive iterative finite-element methods to solve the 2D diffusion equation $\partial\rho(x,y)/\partial t = -C\nabla^2\rho(x,y)$ at steady-state [2] with Eq. (8) as a boundary condition. [5] $\rho(x,y)$ is the local adatom concentration and C, for diffusion-limited kinetics, is the surface diffusivity. Island edges are discretized and represented by a finite number of points. At each time step, we solve the steady-state diffusion equation in the region surrounding each island and calculate net diffusive fluxes into or out of each island edge. The corresponding island size is increased or reduced by moving its boundaries normal to the direction of the flux. In the decay curves, the product $C\rho_\infty^{eq}(T_a)$ determines the time over which an island decays and B defines the shape of the decay curve at small island sizes [12]. It is important to note that the only two unknown parameters in the calculation, B and the product $C\rho_\infty^{eq}(T_a)$, can be determined accurately from island coarsening measurements *only* when the argument

[5] In our analysis, we assume that Eq. (8), applicable only for equilibrium island shapes, is also valid for smaller islands that decay.

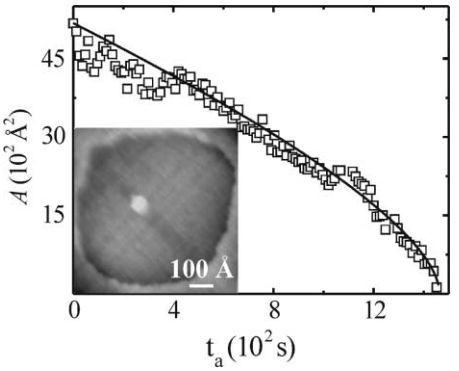

Fig. 3. Measured (open squares) island areas A vs. annealing time t_a for a 2D TiN(0 0 1) adatom island in a vacancy pit during annealing at 1140 K. The solid line is the calculated curve obtained using diffusion-limited model with $B = 0.23$ eV/Å. An STM image (705×715 Å^2) of the island geometry is given in the inset.

of the exponential, $\exp(B\Omega/R_{avg}kT_a)$, in Eq. (9) is such that $(B\Omega/R_{avg}kT_a) \gg 1$. For $(B\Omega/R_{avg}kT_a) \ll 1$, the exponential can be expanded to first order which yields the mean-field expression where $BC\rho_\infty^{eq}(T_a)$ is a single parameter [22,23]. Experimental data, at seven different annealing temperatures, $T_a = 1023$–1223 K, for islands that satisfy the condition $(B\Omega/R_{avg}kT_a) \gg 1$, were fit with calculated results to determine B and $C\rho_\infty^{eq}(T_a)$.

Fig. 3 shows a typical plot of measured (open squares) and calculated (solid line) island area A as a function of annealing time t_a, in this case for a 40 Å adatom island at $T_a = 1140$ K. Decay curves for 14 different adatom islands were equally well fit with $B = 0.23 \pm 0.05$ eV/Å. Combining this result with the measured equilibrium shape in Fig. 2, we obtain, using Eq. (7a), size-dependent λ values. Substituting λ into Eq. (2a), we then determine absolute values for $\beta(\varphi)$. $\kappa(\theta)$ values were calculated for the island in Fig. 1 using the $R(\theta)$ fit obtained from Eq. (1). This yields, from Eq. (6), absolute values for $\tilde{\beta}(\varphi)$. Both β (dashed line) and $\tilde{\beta}$ (solid line) for TiN(0 0 1) are plotted in Fig. 4 as a function of φ. For the two high-symmetry $\langle 1\,1\,0\rangle$ and $\langle 1\,0\,0\rangle$ steps we obtain: $\beta_{1\,1\,0} = 0.21 \pm 0.05$, $\tilde{\beta}_{1\,1\,0} = 0.9 \pm 0.2$ eV/Å, $\beta_{1\,0\,0} = 0.25 \pm 0.05$ eV/Å, and $\tilde{\beta}_{1\,0\,0} = 0.07 \pm 0.02$ eV/Å.

In the unrestricted terrace-step-kink model, $\tilde{\beta}$ is related to the kink formation energy ε on a step as [24]

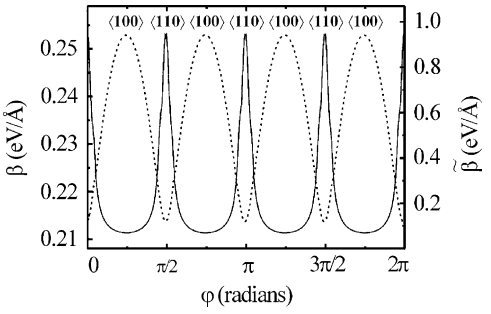

Fig. 4. Absolute values of β vs. φ (dashed line) and $\tilde{\beta}$ vs. φ (solid line) for TiN(0 0 1).

$$\tilde{\beta} = (2a_{\parallel}k_{B}T/a_{\perp}^{2})\sinh^{2}(\varepsilon/2k_{B}T), \quad (10)$$

where $a_{\parallel}$ and $a_{\perp}$ are the unit lattice spacing parallel and orthogonal to the step edge respectively. With $a_{\parallel} = a_{\perp} = 2.12\sqrt{2}$ Å for $\langle 1\,1\,0\rangle$ steps and $a_{\parallel} = 4.24$ Å and $a_{\perp} = 2.12$ Å for $\langle 1\,0\,0\rangle$ steps, we obtain $\varepsilon_{1\,1\,0} = 0.40 \pm 0.02$ eV and $\varepsilon_{1\,0\,0} = 0.11 \pm 0.01$ eV. Since the kink energy results are model-dependent [24,25], however, these values should only be considered as approximate. We have ignored entropic step energy contributions, $(k_{B}T/a_{\parallel}) \times \ln[\coth(\varepsilon/2k_{B}T)]$ [24], to the step energies, which we estimate to be $\simeq -8 \times 10^{-4}$ and -0.02 eV/Å corresponding to ε values of 0.40 and 0.11 eV, respectively, at 1140 K. These values are smaller than the statistical uncertainties in determining β, 0.05 eV/Å for both $\langle 1\,0\,0\rangle$ and $\langle 1\,1\,0\rangle$ steps.

In conclusion, we have shown that island decay measurements in combination with analyses of 2D equilibrium island shapes can be used to determine absolute orientation-dependent step energies on anisotropic, as well as, isotropic surfaces. We used in situ high-temperature (1030–1185 K) STM to determine 2D TiN(0 0 1) vacancy island shapes. Relative orientation-dependent step energies were obtained from inverse Legendre transformation of the equilibrium island shapes. These results were then used in combination with diffusion-limited TiN(0 0 1) adatom island coarsening measurements to obtain absolute orientation-dependent step energies. TiN(0 0 1) islands are found to be anisotropic with $\beta_{1\,1\,0}/\beta_{1\,0\,0} = 0.84$ at $T_{a} = 1140$ K ($\simeq 0.36\ T_{m}$ [26]). We obtain step energies $\beta_{1\,1\,0} = 0.21 \pm 0.05$ eV/Å and $\beta_{1\,0\,0} = 0.25 \pm 0.05$ eV/Å, step stiffnesses $\tilde{\beta}_{1\,1\,0} = 0.9 \pm 0.2$ eV/Å and $\tilde{\beta}_{1\,0\,0} = 0.07 \pm 0.02$ eV/Å, and kink formation energies $\varepsilon_{1\,1\,0} = 0.40$ eV and $\varepsilon_{1\,0\,0} = 0.11$ eV.

Acknowledgements

The authors gratefully acknowledge the financial support of the US Department of Energy (DOE), Division of Materials Science, under contract no. DEFG02-91ER45439 through the University of Illinois Frederick Seitz Materials Research Laboratory (FS-MRL). SVK is supported by NSF under contract no. DMR97-03906. We also appreciate the use of the facilities in the Center for Microanalysis of Materials, partially supported by DOE, at the FS-MRL. We are grateful to M. Giesen and T.L. Einstein for stimulating discussions and insightful comments on the manuscript.

References

[1] F.H. Baumann, D.L. Chopp, T. Díaz de la Rubia, G.H. Gilmer, J.E. Greene, H. Huang, S. Kodambaka, P. O'Sullivan, I. Petrov, MRS Bull. 26 (2001) 182.
[2] S. Kodambaka, V. Petrova, A. Vailionis, P. Desjardins, D.G. Cahill, I. Petrov, J.E. Greene, Surf. Rev. Lett. 7 (2000) 589.
[3] S. Kodambaka, V. Petrova, A. Vailionis, P. Desjardins, D.G. Cahill, I. Petrov, J.E. Greene, Thin Solid Films 392 (2001) 164.
[4] S. Kodambaka, V. Petrova, S.V. Khare, D. Gall, A. Rockett, I. Petrov, J.E. Greene, in preparation.
[5] W.W. Mullins, Interf. Sci. 9 (2001) 9.
[6] N.C. Bartelt, R.M. Tromp, E.D. Williams, Phys. Rev. Lett. 73 (1994) 1656.
[7] K. Arenhold, S. Surnev, H.P. Bonzel, P. Wynblatt, Surf. Sci. 424 (1999) 271;
H.P. Bonzel, A. Emundts, Phys. Rev. Lett. 84 (2000) 5804.
[8] G.S. Icking-Konert, M. Giesen, H. Ibach, Phys. Rev. Lett. 83 (1999) 3880;
M. Giesen, C. Steimer, H. Ibach, Surf. Sci. 471 (2001) 80.
[9] A. Emundts, M. Nowicki, H.P. Bonzel, Surf. Sci. 496 (2002) L35.
[10] S. Kodambaka, V. Petrova, S.V. Khare, D.D. Johnson, I. Petrov, J.E. Greene, Phys. Rev. Lett. 88 (2002) 146101.
[11] D.C. Schlößer, L.K. Verheij, G. Rosenfeld, G. Comsa, Phys. Rev. Lett. 82 (1999) 3843;
C. Steimer, M. Giesen, L. Verheij, H. Ibach, Phys. Rev. B 64 (2001) 85416.

[12] K. Morgenstern, G. Rosenfeld, G. Comsa, Phys. Rev. Lett. 76 (1996) 2113;
K. Morgenstern, G. Rosenfeld, E. Lægsgaard, F. Besenbacher, G. Comsa, Phys. Rev. Lett. 80 (1998) 556.
[13] G.S. Icking-Konert, M. Geisen, H. Ibach, Surf. Sci. 398 (1998) 37.
[14] J.E. Greene, J.-E. Sundgren, L. Hultman, I. Petrov, D.B. Bergstrom, Appl. Phys. Lett. 67 (1995) 2928.
[15] I. Petrov, F. Adibi, J.E. Greene, W.D. Sproul, W.-D. Münz, J. Vac. Sci. Technol. A 10 (1992) 3283.
[16] K. Zeng, R. Schmid-Fetzer, Z. Metallkd. 87 (1996) 540.
[17] Inorganic Index to Powder Diffraction File, Joint Committee on Powder Diffraction Standards, Pennsylvania, 1997, Card numbers 38-1420 and 08-0117 for TiN and TiO respectively.
[18] Image SXM, developed by Prof. Steve Barrett, Liverpool, UK. Available from <http://reg.ssci.liv.ac.uk>.
[19] C. Herring, in: W.E. Kingston (Ed.), The Physics of Powder Metallurgy, McGraw-Hill, New York, 1951, p. 143.
[20] Appendix of S.V. Khare, T.L. Einstein, Phys. Rev. B 54 (1996) 11752.
[21] M. Giesen, Prog. Surf. Sci. 68 (2001) 1.
[22] J.G. McLean, B. Krishnamachari, D.R. Peale, E. Chason, J.P. Sethna, B.H. Cooper, Phys. Rev. B 55 (1997) 1811.
[23] I.M. Lifshitz, V.V. Slyozov, J. Phys. Chem. Solids 19 (1961) 35.
[24] N.C. Bartelt, T.L. Einstein, E.D. Williams, Surf. Sci. 276 (1992) 308.
[25] E.D. Williams, R.J. Phaneuf, J. Wei, N.C. Bartelt, T.L. Einstein, Surf. Sci. 294 (1993) 219.
[26] CRC Handbook of Chemistry and Physics, 82nd ed., 2001–2002, pp. 4–91.